



Cite this: *Mol. Syst. Des. Eng.*, 2023, 8, 586

Received 28th December 2022,  
Accepted 5th April 2023

DOI: 10.1039/d2me00280a

rsc.li/molecular-engineering

We report on the solvent-free synthesis of the perfluorinated analogue of the well-known breathing metal-organic framework MIL-53(Al), *i.e.*, F<sub>4</sub>-MIL-53(Al), featuring tetrafluoroterephthalic acid as linker. The crystal structure was solved and refined from powder X-ray diffraction data and confirmed to be isoreticular with MIL-53(Al). As already reported for the MIL-53(Al) analogue, F<sub>4</sub>-MIL-53(Al) displays a peculiar breathing effect solely induced by the temperature; however, in the latter case the transition occurs with almost no hysteresis and fast kinetics. This unique behavior is reported here for the first time and experimentally demonstrated using differential scanning calorimetry and variable temperature X-ray diffraction.

The development of clean and sustainable methodologies for the large scale synthesis of metal-organic frameworks (MOFs) is a challenge attracting wide scientific interest.<sup>1</sup> Traditional protocols for MOF preparation often need the use of dipolar aprotic solvents such as *N,N*-dimethylformamide (DMF) or *N,N*-dimethylacetamide (DMA), that present a harmful ecotoxicological profile and, for this reason, are restricted by the European Chemicals Agency (ECHA).<sup>2</sup> Even with the use of more sustainable media (*e.g.*, water, acetonitrile or biomasses derived media),<sup>3,4</sup> solvents represent one of the main costs and the main sources of waste in MOFs synthesis. In addition, their recycling is not straightforward, often due to the presence of unreacted

## Solvent-free synthesis of a new perfluorinated MIL-53(Al) with a temperature-induced breathing effect†

Diletta Morelli Venturi, <sup>a</sup> Virginia Guiotto, <sup>b</sup> Roberto D'Amato, <sup>a</sup> Lucia Calucci, <sup>c</sup> Matteo Signorile, <sup>b</sup> Marco Taddei, <sup>d</sup> Valentina Crocellà <sup>b</sup> and Ferdinando Costantino <sup>a</sup>

### Design, System, Application

The current paper deals with the preparation, *via* a solvent-free methodology, of a novel perfluorinated Al-MOF with MIL-53(Al) topology based on tetrafluoroterephthalic acid (H<sub>2</sub>-F<sub>4</sub>BDC). The MOF is constituted of infinite AlO<sub>6</sub> 1D units which design rhombic channels running along the *c*-axis. The synthetic conditions were very simple and they did not need the use of any solvent except methanol and water for the washing. Gas sorption analysis was carried out indicating a microporous structure with BET surface area higher than 1000 m<sup>2</sup> g<sup>-1</sup>. Temperature dependent X-ray powder diffraction coupled with DSC analysis revealed the presence of a narrow pore to large pore reversible phase transition purely induced by temperature which is rarely observed on this kind of materials.

species or by-products.<sup>5</sup> An effective way to design cheaper and efficient protocols for the preparation of MOFs includes solvent-free syntheses, although the complete elimination of the reaction media is often not trivial. Mechanochemistry, accelerated aging and “shake n' bake” are some of such synthetic strategies frequently used for achieving MOFs of good quality.<sup>6</sup>

Aluminum is one of the cheapest and most abundant metals present in nature (8.2 wt% on the earth crust).<sup>7</sup> The interest for this metal as inorganic node in MOFs has seen a rapid growth in the last decade, as a large variety of Al-MOFs<sup>8–13</sup> were reported in the literature. These MOFs usually display high stability and find application in atmospheric water harvesting,<sup>14</sup> gas separation,<sup>15</sup> adsorption-driven heat pumps<sup>16–18</sup> and molecules sorption in solution.<sup>19</sup> Since their first appearance in the literature, there is a particular interest on MOFs with the MIL-53 topology and on their breathing behaviour due to their high stability and good gas loading capacity and their performance in the separation of CO<sub>2</sub>.<sup>6</sup>

Perfluorinated linkers bearing electron-withdrawing atoms can strongly interact with molecules having quadrupole moments like CO<sub>2</sub>, thus increasing the affinity with the probe.<sup>13</sup> We have already used perfluorinated linkers for the synthesis of MOFs such as UiO-66(Ce),<sup>20</sup> MIL-140(Ce),<sup>20</sup>

<sup>a</sup> Department of Chemistry, Biology and Biotechnology, Università degli Studi di Perugia, Via Elce di Sotto, 8 – 06123 Perugia, Italy. E-mail: ferdinando.costantino@unipg.it

<sup>b</sup> Department of Chemistry, NIS and INSTM Centers, Università di Torino, Via G. Quarollo 15 and Via P. Giuria 7, 10125, Turin, Italy. E-mail: valentina.crocella@unito.it

<sup>c</sup> ICCOM-CNR, Via G. Moruzzi 1, 56124 Pisa, Italy

<sup>d</sup> Department of Chemistry and Industrial Chemistry, Università di Pisa, Via Giuseppe Moruzzi 13, 56124, Pisa, Italy

† Electronic supplementary information (ESI) available: Synthetic procedures, instrumental details, Rietveld refinement details, SEM images, additional SS-NMR spectra, VT-XRPD patterns. CCDC 2215705 contains the crystallographic data for F<sub>4</sub>-MIL53(Al). For ESI and crystallographic data in CIF or other electronic format see DOI: <https://doi.org/10.1039/d2me00280a>

‡ These authors contributed equally.



MOF-801(Zr).<sup>21</sup> Tetrafluoroterephthalic acid ( $H_2F_4BDC$ ) has been recently used as linker for the synthesis of several MOFs<sup>20,22</sup> showing peculiar gas sorption behaviour. Among them,  $F_4\text{-IL-140A(Ce)}$  displays an interesting S-shaped  $CO_2$  adsorption isotherm at room temperature, responsible for a high  $CO_2/N_2$  IAST selectivity.<sup>20</sup> Moreover, in  $F_4\text{-MIL-140A(Ce)}$ , guest molecules induce the rotation of the aromatic rings, whereas this effect is not reported in the non-fluorinated analogue.<sup>20</sup> In this work, we focus on fluorinated Al-based MOFs and we present a simple strategy for the solvent-free synthesis of the perfluorinated analogue of MIL-53(Al) (hereafter  $F_4\text{-MIL-53(Al)}$ ) starting from  $H_2F_4BDC$  and  $Al(NO_3)_3 \cdot 9H_2O$  as precursors.

$F_4\text{-MIL-53(Al)}$  was synthesized by mixing the powders of the two reagents in equimolar ratio in a Teflon reactor and heating at 120 °C for 24 h. The synthetic procedure did not need any kind of solvent, other than the hydration water contained in the metal precursor. A microcrystalline product was obtained and the unreacted reagents were washed with water and acetone. The crystal structure, solved *ab initio* from powder X-ray diffraction (PXRD) data and refined with the Rietveld method (Fig. 1), displays orthorhombic symmetry (space group *Imma*) with  $a = 6.6305(15)$  Å,  $b = 18.117(5)$  Å, and  $c = 10.748(3)$  Å as lattice parameters (all refinement details in ESI†).  $F_4\text{-MIL-53(Al)}$  exhibits the well-known structure of the MIL-53 MOFs family: the framework is constituted of 1D chains running along the  $a$ -axis and built from OH corner-sharing  $[AlO_4(OH)_2]$  octahedra connected by  $F_4BDC$  linkers (Fig. 1). The aromatic rings are disordered, and they were refined over two equivalent tilted positions with 50% occupancy each. The two carboxylate moieties of each  $F_4BDC$  are linked to different aluminium cations with an interatomic distance that is typical of Al–O bond in octahedra (1.8–2 Å). C–C, C–F, and C–O distances of the linker are 1.4–1.5 Å, 1.3 Å, and 1.2 Å, respectively.

Argon adsorption analysis was performed at 87 K to evaluate the specific surface area (SSA) of  $F_4\text{-MIL-53(Al)}$ . The isotherm shows a type I(a) profile (Fig. S4†) according to the IUPAC classification, characteristic of materials having micropores of width <1 nm.<sup>23</sup> The resulting SSA is 1042 m<sup>2</sup> g<sup>-1</sup>, lower than that reported for MIL-53(Al), measured using the same adsorbate (1480 m<sup>2</sup> g<sup>-1</sup>).<sup>24</sup> This can be attributed to the presence of a heavier and bulkier linker in  $F_4\text{-MIL-53(Al)}$ .

The local structure of  $F_4\text{-MIL-53(Al)}$  was further investigated by multinuclear ( $^1H$ ,  $^{19}F$ ,  $^{13}C$ , and  $^{27}Al$ ) solid state nuclear magnetic resonance (SS-NMR) spectroscopy. The  $^1H$  spectrum of  $F_4\text{-MIL-53(Al)}$ , acquired by direct excitation (DE) under spinning at the magic angle (MAS), shows a peak at 3.2 ppm (Fig. 2a) ascribable to  $\mu_2\text{-OH}$  groups. The observed chemical shift is slightly higher than that reported for MIL-53(Al).<sup>25–27</sup> No signals arising from carboxylic acid groups of residual  $H_2F_4BDC$  are detected in the spectrum. A single signal is observed also for fluorine atoms on  $F_4BDC$  linkers in the  $^{19}F$  DE-MAS spectrum, with a wide spinning side band pattern arising from fluorine chemical shift anisotropy (Fig. S5†) and an isotropic signal centred at -145.0 ppm (Fig. 2b). The  $^{19}F\text{-}^{13}C$  cross-polarization (CP) MAS spectrum (Fig. 2c) shows three sharp signals at 117.2, 145.4, and 166.3 ppm ascribable to quaternary, fluorinated and carboxylic carbons of  $F_4BDC$ , respectively, confirming that no unreacted linker is present in the sample. In the  $^{27}Al$  DE-MAS spectrum (Fig. 2d), a signal typical of Al atoms in an octahedral environment is observed, arising from  $[AlO_4(OH)_2]$  centres. The chemical shift and quadrupolar interaction parameters obtained by an analysis of the spectral line shape ( $\delta = 3.9$  ppm,  $C_Q = 9.46$  MHz, and  $\eta_Q = 0$ ; Fig. S6†) are similar to those reported for the high temperature (I<sub>p</sub>) phase of MIL-53(Al),<sup>26–29</sup> although with a larger value of the quadrupolar coupling constant  $C_Q$ , indicating that a higher electric field gradient is experienced

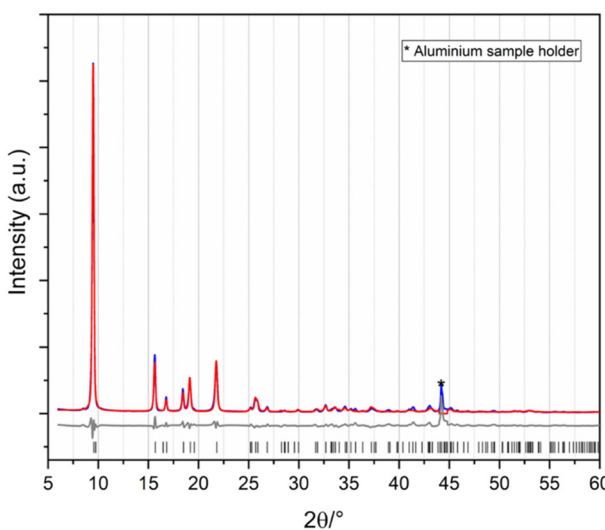


Fig. 1 Left: Rietveld refinement of  $F_4\text{-MIL-53(Al)}$ . The experimental PXRD pattern is shown in blue, the calculated in red and the difference (experimental – calculated) is given in grey. The allowed reflection positions are given in black. Right: Crystal structure of  $F_4\text{-MIL-53(Al)}$ . Colour code: aluminium (blue), carbon (grey), oxygen (red) and fluorine (green).



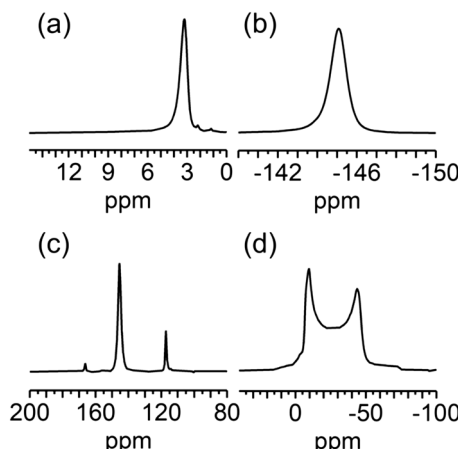


Fig. 2 (a)  $^1\text{H}$  DE-MAS-NMR, (b)  $^{19}\text{F}$  DE-MAS-NMR, (c)  $^{19}\text{F}$ - $^{13}\text{C}$  CP-MAS-NMR, and (d)  $^{27}\text{Al}$  DE-MAS-NMR spectra of  $\text{F}_4\text{-MIL-53(Al)}$ .

by the Al nuclei bound to  $\text{F}_4\text{BDC}$  linkers. It must be pointed out that an effect on  $C_Q$  has been reported upon functionalization of BDC linkers.<sup>25</sup> On the other hand,  $\eta_Q = 0$  is a hint of high local symmetry for Al centers in  $\text{F}_4\text{-MIL-53(Al)}$ , in agreement with their location on a special position with Wickoff symbol 4d and site symmetry  $2/m$ .

The thermogravimetric analysis (TGA) (Fig. S7†) shows a weight loss of about 3% between 25 and 200 °C, attributed to residual water loss. The decomposition of the framework starts at 450 °C with a steep weight loss of 80% and, up to the end of the analysis, no other significant weight losses are observed. Experimental data and theoretical molecular formula are in good agreement (calcd 70%, obs 80%) and lead to a formula  $\text{Al(OH)(F}_4\text{BDC)}\cdot 0.4\text{H}_2\text{O}$ . The presence of a small amount of physisorbed water (interacting *via* hydrogen

bonding with the structural OH groups) is also suggested by the IR spectra of the as synthesized sample, characterized by a weak and broad component between 3500 and 3200  $\text{cm}^{-1}$ , ascribed to the stretching vibrations of hydrogen-bonded OH species; this water is then easily removed by simply outgassing the sample at room temperature (Fig. S8†). A detailed description of the IR spectra of  $\text{F}_4\text{-MIL-53(Al)}$  is reported in the ESI.†

Variable temperature-PXRD (VT-PXRD) patterns were collected between 25 and 240 °C (Fig. 3 – left and S9†) to investigate the effect of temperature variations on the structure of  $\text{F}_4\text{-MIL-53(Al)}$ . A phase transition starting at 180 °C is observed, when a shoulder at  $8.60^\circ 2\theta$  close to the main reflection ( $9.70^\circ 2\theta$ ) arises, indicating the formation of a large pore (lp) phase. This phenomenon could be related to an initial (but not total) breathing effect induced by the removal of the small and weak interacting amount of water present in the pristine material, already highlighted by the IR spectra and by the TG analysis (which shows the loss of this water within 200 °C – see Fig. S7 and S8†). Above 200 °C, therefore, the material is totally anhydrous, but still increasing the temperature to 240 °C, the XRD pattern totally evolves towards the lp phase. In Table S2† the comparison between the lattice parameters of  $\text{F}_4\text{-MIL-53(Al)}$  obtained from Rietveld refinement of the initial structure and those obtained from Pawley fit of the material at 240 °C is shown (Fig. S10†). Moving from the np to the lp phase, the unit cell volume changes from 1292.1 to 1482  $\text{\AA}^3$ , corresponding to a 14.7% increase. In comparison, the np to lp phase transition in  $\text{MIL-53(Al)}$ , which occurs only in response to the loss of adsorbed water at elevated temperature, involves a unit cell volume change from 946.74 to 1411.84  $\text{\AA}^3$ , corresponding to a 49.1% increase.<sup>30</sup> This is mainly due to the much lower

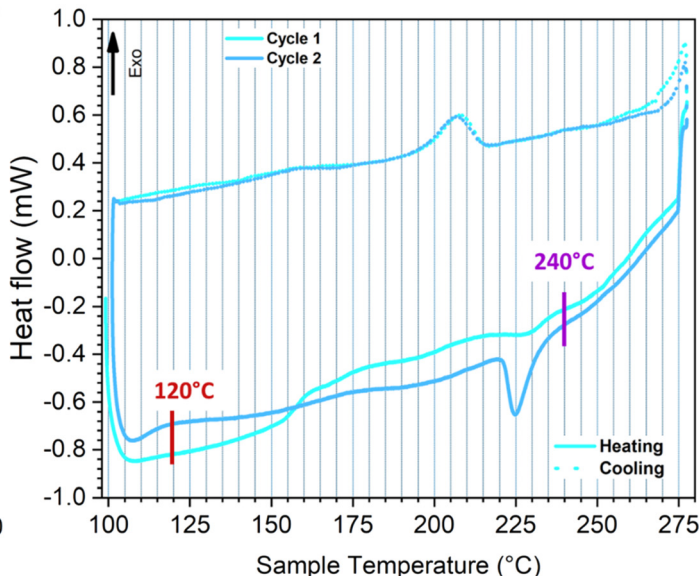
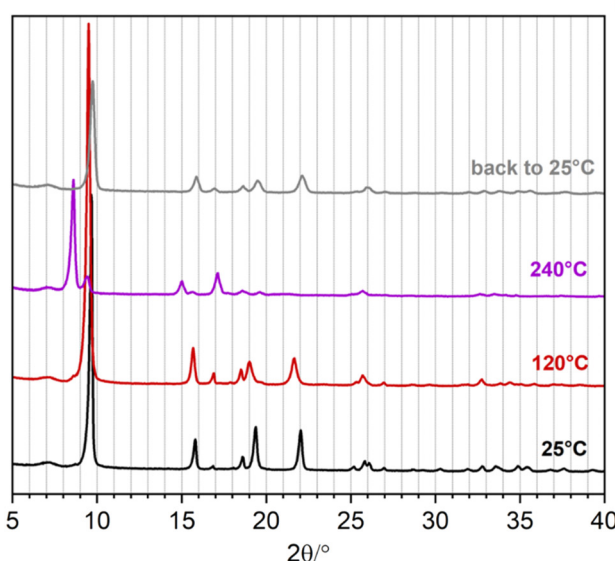


Fig. 3 VT-XRD patterns of  $\text{F}_4\text{-MIL-53(Al)}$  at room temperature (25 °C – black), before the phase transition (120 °C red), after the phase transition (240 °C purple) and after returning to the room temperature (25 °C – light grey) (left). DSC profile of  $\text{F}_4\text{-MIL-53(Al)}$  (right): first cycle (cyan) and second cycle (light blue). Full and dotted curves refer to the heating and cooling cycles respectively (right).



volume of the np phase in the case of MIL-53(Al), compared to  $F_4$ -MIL-53(Al), where the steric hindrance of the perfluorinated rings probably prevents the structure from reaching a more compact form.  $F_4$ -MIL-53(Al) goes back to the initial, narrow pore (np) phase when the temperature is brought back to RT.

Since the XRD measurement detects a complete structural variation well above 200 °C, on an already anhydrous material, we hypothesise that the observed np → lp transition could not to be ascribed to the desorption of water, as instead observed for MIL-53(Al).<sup>30</sup> Rather, we explain the phenomenon as a rare case of purely temperature-dependent breathing. This initial interpretation is definitely confirmed by differential scanning calorimetry (DSC) (Fig. 3 – right). These measurements were performed at temperature higher than 100 °C to avoid any possible water contamination during the cooling cycles. The first heating cycle (full cyan curve) does not exhibit any well-defined endothermic peak below 200 °C, due to a gradual removal of the residual adsorbed water, probably accompanied by a partial np → lp transition, as detected by the VT-PXRD analysis. Above 200 °C, a weak endothermic peak is observable at around 230 °C, testifying the definitive structural variation to the lp phase, in analogy with the evolution of the diffraction pattern (purple curve in Fig. 3 – left). The first cooling cycle (dotted cyan curve) instead shows a rather sharp exothermic peak ( $T_{\text{onset}} = 216.8$  °C) generated by a lp → np phase transition that occurs in totally anhydrous conditions. The definitive proof of the purely temperature-dependent breathing is given by the second heating–cooling cycle (recorded on a totally water-free material) which exhibits a sharp endothermic peak well above 200 °C ( $T_{\text{onset}} = 221.9$  °C) and a corresponding exothermic signal ( $T_{\text{onset}} = 216.8$  °C) in the cooling profile, generated by the thermal induced np → lp and lp → np transitions respectively. A third heating–cooling cycle, exhibiting the same thermal events of the second one, was collected to reveal the complete reproducibility and reversibility of such thermal-induced phenomenon (Fig. S11†). The temperature at which the endothermic phenomenon takes place corresponds to the evolution of the diffraction patterns from np to lp revealed by VT-PXRD, suggesting that we can directly measure the heat involved in the thermal breathing (values reported in Table 1). The 6.85 J g<sup>-1</sup> absorbed during the np → lp transition corresponds to 1.9 kJ mol<sup>-1</sup>. This value is lower than the one reported by Llewellyn *et al.* for the np → lp transition in MIL-53(Cr),<sup>31,32</sup> due probably to the lower variation of volume in  $F_4$ -MIL-

53(Al), as the nature of the metal was found not to have an effect on the energetics of breathing.<sup>31,32</sup> The slightly different temperatures at which the transition occurs during heating and cooling suggest that there is a small hysteresis, analogous to what observed for adsorption-induced breathing in MIL-53(Al). Many works in the literature report the breathing behavior of MIL-53 induced by the hydration/dehydration of the structure. It is worth noting a recent work by Liang *et al.* in which the removal of coordinated water molecules occurs upon a high temperature treatment.<sup>33</sup> The authors define such mechanism “temperature-induced”, but in their system the adsorption and desorption of water is actually involved in the breathing process. On the other hand, Liu *et al.* reported that MIL-53(Al) is able to undergo a structural modification as a function of temperature without the aid of guest molecules, but with a pronounced temperature hysteresis (almost 200 °C between np and lp). In this case, the transition can be observed upon a temperature program keeping the sample under vacuum.<sup>34</sup>

The very small hysteresis (lower than 5 °C) and the fast kinetics associated to the structural rearrangement render  $F_4$ -MIL-53(Al) a unique example of a thermo-responsive MOF.<sup>35</sup>

## Conclusions

In this paper, a new Al-based MOF built with tetrafluoro terephthalic acid as linker and displaying a MIL-53 topology was synthesized with a simple solvent free procedure. The structure was solved and refined from PXRD data. The new material was characterized with TG analysis, Ar adsorption at 87 K, SS-NMR and *in situ* IR spectroscopy. A VT-PXRD study reveals the presence of a reversible phase transition induced by temperature above 200 °C (*i.e.* in anhydrous conditions). The actual nature of this reversible temperature-induced phase transition was confirmed by DSC analysis. This peculiar behavior will deserve further experimental investigation coupled with computational modelling, to possibly disclose the mechanism of the associated structural rearrangement, not induced by the simple desorption of molecules. Finally, a complete analysis of the sorption behaviour of this new MOF is currently in progress. Preliminary data reveal that  $F_4$ -MIL-53(Al) undergoes structural changes also upon adsorption–desorption of different probes, including water, nitrogen and carbon dioxide. Further measurements coupled with modeling approaches will be fundamental to really understand the causes that promote the structural changes of this MOF induced by both temperature and interaction with several adsorbates.

## Author contributions

D. M. V. – investigation, data curation, writing – original draft, writing – review & editing. V. G. – investigation, data curation, writing – original draft, writing – review & editing. R. D. – conceptualization. L. C. – Investigation, data curation,

**Table 1** Main details of the DSC signals related to the second heating–cooling cycle

	Cycle 2				
	$T_{\text{onset}}$ (°C)	$T_{\text{off}}$ (°C)	$\Delta(t_{\text{on}} - t_{\text{off}})$ (min)	Heat (J g <sup>-1</sup> )	Peak maximum (°C)
Heating	221.9	230.4	28	+6.85	225.07
Cooling	216.8	202.3	51	-6.00	206.29



writing – original draft, writing – review & editing. M. T. data curation writing – review & editing. M. S. writing – review & editing. F. C. and V. C. – conceptualization, project administration, supervision, writing – review & editing.

## Conflicts of interest

“There are no conflicts to declare”.

## Acknowledgements

F. C. thanks Dr Andrea Ienco (CNR-ICCOM) for performing VT-PXRD measurements. All the authors acknowledge the Italian MUR through the Project PRIN 2020 doMino (ref 2020P9KBKZ). CISUP (University of Pisa) is acknowledged for the use of the Bruker Avance Neo 500 Solid State NMR Spectrometer. Dr. Francois-Xavier Coudert (CNRS/Chimie ParisTech) is acknowledged for helpful discussion about temperature-induced breathing phenomena.

## Notes and references

- 1 S. Wang and C. Serre, *ACS Sustainable Chem. Eng.*, 2019, **7**, 11911–11927.
- 2 <https://eur-lex.europa.eu/legal-content/EN/TXT/?uri=celex%3A32009L0032>.
- 3 D. Morelli Venturi, F. Campana, F. Marmottini, F. Costantino and L. Vaccaro, *ACS Sustainable Chem. Eng.*, 2020, **8**, 17154–17164.
- 4 S. Leubner, R. Stäglich, J. Franke, J. Jacobsen, J. Gosch, Renøes, H. Reinsch, G. Aurin, Jürgens, P. Y. Ot and N. Stock, *Chem. – Eur. J.*, 2020, **26**, 3877–3883.
- 5 E. S. M. El-Sayed and D. Yuan, *Green Chem.*, 2020, **22**, 4082–4104.
- 6 C. Serre, F. Millange, C. Thouvenot, M. Noguès, G. Marsolier, D. Louër and G. Férey, *J. Am. Chem. Soc.*, 2002, **124**, 13519–13526.
- 7 Y. Liu, Y. Li, F. Zuo, J. Liu, Y. Xu, L. Yang, H. Zhang, H. Wang, X. Zhang, C. Liu, Q. Li and H. Li, *Small*, 2022, **18**, 2203236.
- 8 N. Tannert, C. Jansen, S. Nießing and C. Janiak, *Dalton Trans.*, 2019, **48**, 2967–2976.
- 9 H. Reinsch, M. A. van der Veen, B. Gil, B. Marszalek, T. Verbiest, D. de Vos and N. Stock, *Chem. Mater.*, 2013, **25**, 17–26.
- 10 T. Steenhaut, Y. Filinchuk and S. Hermans, *J. Mater. Chem. A*, 2021, **9**, 21483–21509.
- 11 J. Li, M. J. Hurlock, V. G. Goncharov, X. Li, X. Guo and Q. Zhang, *Inorg. Chem.*, 2021, **60**, 4623–4632.
- 12 A. Knebel, S. Friebe, N. C. Bigall, M. Benzaqui, C. Serre and J. Caro, *ACS Appl. Mater. Interfaces*, 2016, **8**, 7536–7544.
- 13 A. E. Amooghin, H. Sanaeepur, R. Luque, H. Garcia and C. Banglin, *Chem. Soc. Rev.*, 2022, **51**, 7427–7508.
- 14 W. Xu and O. M. Yaghi, *ACS Cent. Sci.*, 2020, **6**, 1348–1354.
- 15 A. López-Olvera, J. A. Zárate, E. Martínez-Ahumada, D. Fan, M. L. Díaz-Ramírez, P. A. Sáenz-Cavazos, V. Martis, D. R. Williams, E. Sánchez-González, G. Maurin and I. A. Ibarra, *ACS Appl. Mater. Interfaces*, 2021, **13**, 39363–39370.
- 16 D. Lenzen, J. Zhao, S. J. Ernst, M. Wahiduzzaman, A. Ken Inge, D. Fröhlich, H. Xu, H. J. Bart, C. Janiak, S. Henninger, G. Maurin, X. Zou and N. Stock, *Nat. Commun.*, 2019, **10**, 3025.
- 17 T. J. Matemb Ma Ntep, H. Reinsch, P. P. C. Hügenell, S. J. Ernst, E. Hastürk and C. Janiak, *J. Mater. Chem. A*, 2019, **7**, 24973–24981.
- 18 A. Cadiau, J. S. Lee, D. Damasceno Borges, P. Fabry, T. Devic, M. T. Wharmby, C. Martineau, D. Foucher, F. Taulelle, C. H. Jun, Y. K. Hwang, N. Stock, M. F. de Lange, F. Kapteijn, J. Gascon, G. Maurin, J. S. Chang and C. Serre, *Adv. Mater.*, 2015, **27**, 4775–4780.
- 19 A. Samokhvalov, *Coord. Chem. Rev.*, 2018, **374**, 236–253.
- 20 R. D'Amato, A. Donnadio, M. Carta, C. Sangregorio, D. Tiana, R. Vivani, M. Taddei and F. Costantino, *ACS Sustainable Chem. Eng.*, 2019, **7**, 394–402.
- 21 D. Morelli Venturi, M. S. Notari, R. Bondi, E. Mosconi, W. Kaiser, G. Mercuri, G. Giambastiani, A. Rossin, M. Taddei and F. Costantino, *ACS Appl. Mater. Interfaces*, 2022, **14**(36), 40801–40811.
- 22 R. D. Amato, R. Bondi, I. Moghaddas, F. Marmottini, M. J. McPherson, H. Naïli, M. Taddei and F. Costantino, *Inorg. Chem.*, 2021, **60**, 14294–14301.
- 23 M. Thommes, K. Kaneko, A. V. Neimark, J. P. Olivier, F. Rodriguez-Reinoso, J. Rouquerol and K. S. W. Sing, *Pure Appl. Chem.*, 2015, **87**, 1051–1069.
- 24 B. Seoane, S. Sorribas, Á. Mayoral, C. Téllez and J. Coronas, *Microporous Mesoporous Mater.*, 2015, **203**, 17–23.
- 25 Y. Jiang, J. Huang, S. Marx, W. Kleist, M. Hunger and A. Baiker, *J. Phys. Chem. Lett.*, 2010, **1**, 2886–2890.
- 26 C. Lieder, S. Opelt, M. Dyballa, H. Henning, E. Klemm and M. Hunger, *J. Phys. Chem. C*, 2010, **114**, 16596–16602.
- 27 T. Loiseau, C. Serre, C. Huguenard, G. Fink, F. Taulelle, M. Henry, T. Bataille and G. Férey, *Chem. – Eur. J.*, 2004, **10**, 1373–1382.
- 28 A. E. Khudozhitkov, S. S. Arzumanov, A. V. Toktarev, S. V. Cherepanova, A. A. Gabrienko, D. I. Kolokolov and A. G. Stepanov, *Phys. Chem. Chem. Phys.*, 2021, **23**, 18925–18929.
- 29 R. Giovine, C. Volkinger, J. Trébosc, J. P. Amoureux, T. Loiseau, O. Lafon and F. Pourpoint, *Acta Crystallogr., Sect. C: Struct. Chem.*, 2017, **73**, 176–183.
- 30 T. Loiseau, C. Serre, C. Huguenard, G. Fink, F. Taulelle, M. Henry, T. Bataille and G. Férey, *Chem. – Eur. J.*, 2004, **10**, 1373–1382.
- 31 P. L. Llewellyn, G. Maurin, T. Devic, S. Loera-Serna, N. Rosenbach, C. Serre, S. Bourrelly, P. Horejada, Y. Filinchuk and G. Férey, *J. Am. Chem. Soc.*, 2008, **130**, 12808–12814.
- 32 S. Devautour-Vinot, G. Maurin, F. Henn, C. Serre, T. Devic and G. Férey, *Chem. Commun.*, 2009, 2733–2735.
- 33 J. Liang, X. Li, R. Xi, G. Shan, P. Z. Li, J. Liu, Y. Zhao and R. Zou, *ACS Mater. Lett.*, 2020, **2**, 220–226.
- 34 Y. Liu, J.-H. Her, A. Dailly, A. J. Ramirez-Cuesta, D. A. Neumann and C. M. Brown, *J. Am. Chem. Soc.*, 2008, **130**, 11813–11818.
- 35 A. Schneemann, V. Bon, I. Schwedler, I. Senkovska, S. Kaskel and R. A. Fischer, *Chem. Soc. Rev.*, 2014, **43**, 6062–6096.

